nature electronics

ARTICLES

https://doi.org/10.1038/s41928-020-0425-9

A nonlocal spin Hall magnetoresistance in a platinum layer deposited on a magnon junction

C. Y. Guo[1,2,6], C. H. Wan[1,6], W. Q. He[1], M. K. Zhao[1], Z. R. Yan[1], Y. W. Xing[1], X. Wang[1], P. Tang[1], Y. Z. Liu[1], S. Zhang[3], Y. W. Liu[4] and X. F. Han[1,2,5]✉

Magnetoresistance effects are used in a variety of devices including hard disk drives and magnetic random access memories. In particular, giant magnetoresistance and tunnelling magnetoresistance can be used to create spin valves and tunnel junctions in which the resistance depends on the relative magnetization orientations of two ferromagnetic conducting layers. Here, we report a magnetoresistance effect that occurs in a platinum layer deposited on a magnon junction consisting of two insulating magnetic yttrium iron garnet (YIG) layers separated by an antiferromagnetic nickel oxide spacer layer. The resistance of the platinum layer is found to depend on the magnetization of the YIG layer in direct contact with it (an effect known as spin Hall magnetoresistance), but also the magnetization of the adjacent YIG layer in the junction. The resistance of the platinum layer is higher when the two YIG layers are aligned antiparallel than when parallel. We assign this behaviour to a magnonic nonlocal spin Hall magnetoresistance in which spin-carrying magnon propagation across the junction affects spin accumulation at the metal interface and hence modulates the spin Hall magnetoresistance. The effect could be used to develop spintronic and magnonic devices that have spin transport properties controlled by an all-insulating magnon junction and are thus free from Joule heating.

Spintronics uses the spin of electrons to encode, store, process and transmit data and was established on the basis of magneto-transport effects such as giant magnetoresistance (GMR)[1,2] and tunnelling magnetoresistance (TMR)[3,4], which occur in spin valves and magnetic tunnel junctions. These device structures consist of two conductive ferromagnetic layers separated by a non-magnetic metal layer (a spin valve) or an insulator layer (a magnetic tunnel junction). The magnetoresistance causes a relatively low or high resistance state to occur when the two magnetic layers are parallel or antiparallel, respectively. Magnetic tunnel junctions have become key components in hard disk drives[5] and magnetic random access memories (MRAMs) for information storage[6,7].

Like electron spins, magnons (quasiparticles formed from the collective spins of magnetically ordered systems) are capable of transmitting spin angular momenta over long distances. In insulating ferromagnetic[8–12] and antiferromagnetic[13–16] materials, they are the only angular momentum carriers. Notably, unlike electron spins, magnons avoid moving electron charge, so spin propagation is free of Joule heating and is intrinsically energy efficient.

Several magnon-based devices have been proposed and demonstrated[17]. Magnon valves[18] and magnon junctions[16] (MJs) based on yttrium iron garnet ($Y_3Fe_5O_{12}$, YIG), with the structures YIG/Au/YIG and YIG/NiO/YIG, respectively, have been fabricated. With these devices it has been shown that magnon currents can transmit through the entire structure, such that the spin Seebeck signal[19,20] observed at one of the interfaces is either the sum or difference of the contributions from the two magnetic layers, depending on whether the two magnetizations are aligned parallel or antiparallel. More recently, it was reported that precessing YIG at its ferromagnetic resonance in a YIG/CoO/Co spin valve pumps a spin current into the Co layer across the CoO layer, and the magnitude of the inverse spin Hall voltage produced by the spin current depends on the relative orientation of the YIG and Co magnetization[21]. The above magnon valve[18] and the YIG/CoO/Co spin valve structure[21] can function as magnon transistors which control magnon/spin current[22]. Furthermore, another kind of magnon transistor has been demonstrated in which magnon conductance can be effectively modulated by a gate current[22–24] via magnon generation or annihilation[25].

In a bilayer system such as a layer of platinum on YIG, depending on the magnetic orientation of the YIG, there also exists a magnetoresistance effect called the spin Hall magnetoresistance (SMR). An applied current in platinum can generate a spin current with its polarization in the plane of the layer and orthogonal to the applied current (known as the spin Hall effect, SHE)[26,27]. The induced spin current in turn produces a charge current in the direction opposed to the applied current (this is known as the inverse SHE), and so the spin current becomes an additional source of resistance. However, an accumulation of spins can occur near the interface, generating a diffusion spin current that flows opposite to the induced spin current. The net spin current is thus reduced and the resistance is lowered[28,29]. This is the cause of the SMR: when the spin polarization of the spin current is perpendicular to the YIG magnetization, spin accumulation is lowered due to spin-transfer torque and the resistance is thus highest. When the spin polarization of the spin current is parallel to the YIG magnetization, transfer of the electron spin current to the magnon current of YIG occurs[10,22–24,30] and the magnitude of the spin accumulation depends on the detail of the spin conductance of the interface. SMR is considered an interface effect, dependent only on the relative orientation of the electric current and the magnetization at the contact.

In this Article, we show that the resistance of platinum in such heterostructures is dependent on the magnetization direction of

[1]Beijing National Laboratory for Condensed Matter Physics, Institute of Physics, University of Chinese Academy of Sciences, Chinese Academy of Sciences, Beijing, China. [2]Center of Materials Science and Optoelectronics Engineering, University of Chinese Academy of Sciences, Beijing, China. [3]Department of Physics, University of Arizona, Tucson, AZ, USA. [4]School of Physics Science and Engineering, Tongji University, Shanghai, China. [5]Songshan Lake Materials Laboratory, Dongguan, Guangdong, China. [6]These authors contributed equally: C. Y. Guo, C. H. Wan. ✉e-mail: xfhan@iphy.ac.cn

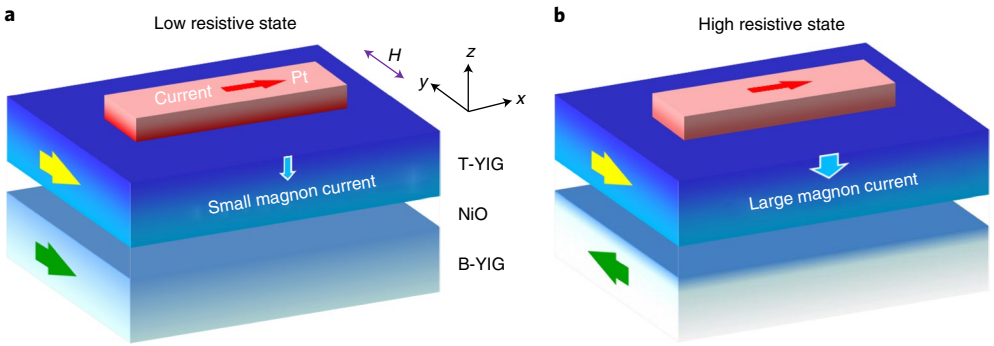

Fig. 1 | Schematics of the YIG/NiO/YIG/Pt heterostructure and the MNSMR effect. a,**b**, Spin (magnon) accumulation in the P (low resistive) state (**a**) and AP (high resistive) state (**b**) is shown schematically with red (blue) scale. Magnetization of the top (T) and bottom (B) YIG layers is represented by yellow and green arrows, respectively. Light blue arrows represent magnon current injected into the T-YIG at the Pt/T-YIG interface. The effective magnon conductance is lower for the P state than for the AP state, leading to a larger spin accumulation at the platinum interface. Consequently, an MNSMR effect occurs where the platinum layer has a lower resistance for the P state than for the AP state.

the contacting YIG, as well as on the magnetization of another YIG layer separated by a NiO spacer (Fig. 1). The orientation of the two YIG magnetizations changes the effective magnon conductance across the junction. In the antiparallel (AP) state, the conductance is higher, leading to lower spin accumulation and a higher resistance in the platinum than in the parallel (P) state. We term this effect the magnonic nonlocal spin Hall magnetoresistance (MNSMR).

Measurement of the spin Seebeck effect and SMR

Figure 2a presents the hysteresis loop of a YIG(100)/NiO(10)/YIG(60 nm) MJ. Sharp transitions indicate the reversal of top (T) and bottom (B) YIG magnetization. Based on our previous work[16], it is known that the B-YIG, which was grown epitaxially on a $Gd_3Ga_5O_{12}$ (GGG) substrate, has smaller coercivity than the T-YIG. Figure 2b shows the resistance change ΔR of a platinum layer on the MJ as a constant magnetic field rotates in three different planes. The applied magnetic field, H, of 1 T completely saturates both YIG layers in the field direction. If applied current, I, flows in the x direction, the SHE dictates that the polarization of spin chemical potential ($\boldsymbol{\mu}_{Pt}$) is along the y axis for the spin current flowing perpendicular to the layers. If H rotates in the xoz plane such that the field is always perpendicular to $\boldsymbol{\mu}_{Pt}$, we find $\Delta R = 0$. When H rotates in the other two planes, the angle between $\boldsymbol{\mu}_{Pt}$ and the YIG magnetization varies and ΔR oscillates with a period of 180°. These observations are standard characteristics of the SMR effect.

To allow the two YIG layers to present a variable relative magnetization direction, we swept a magnetic field H_y along the y axis. We first examined the spin Seebeck effect (SSE) of the described MJs. A temperature gradient was applied perpendicular to the layers by sourcing a heating current (I_{heat}). The voltage (V_{SSE}) on the platinum stripe along the x axis was measured (Fig. 2c), as previously reported[16]. The V_{SSE} signal shows the magnon valve effect and receives contributions from both YIG layers: when the YIG layers are parallel (antiparallel), the magnon current arriving at the platinum layer is the sum (difference) of the magnon currents from the two YIG layers. P and AP states are marked in Fig. 2c by unshaded and shaded regions, respectively. The H_y dependence of V_{SSE} and dV_{SSE}/dH_y clearly captures the coercivity H_c of the MJ. When the NiO spacer has a thickness of 30 nm, the magnon current from the B-YIG decays almost completely in the NiO, and thus reversal of the B-YIG does not affect V_{SSE} (Fig. 2d).

Measurement of the MNSMR of platinum on the magnon junction

The above magnon valve effect unambiguously shows that magnon current is capable of propagating through the entire MJ. To investigate magnetization-dependent magnon transport inside the MJ, we measured the resistance of the platinum layer. As expected from the conventional SMR, the resistance is lowest at a high magnetic field, H_y. When the field reduces, magnetization of the T-YIG gradually deviates from the y direction and the platinum resistance increases. Notably, there is a sharp jump in the resistance, with a typical magnitude of $MR \equiv (R_{AP} - R_P)/R_P$ of 5.1×10^{-4}% at 100 K, at the H_c of the B-YIG (Fig. 3a). For a thicker NiO layer (30 nm), the resistance jump does not occur (Fig. 3b). The H_y dependence of ΔR_{SMR} in Fig. 3a is decomposed into two parts (for details of the decomposition procedure see Supplementary Section 1) and is shown in Fig. 3c. The blue curve represents the conventional SMR of the T-YIG/Pt bilayer. The red curve singles out the response of the resistance jump to the reversal of the B-YIG and has a similar dependence as the GMR and TMR effects.

Elimination of magnetic coupling mechanisms

To address the origin of the resistance jump we first eliminated the possibility of magnetic coupling between the T-YIG and B-YIG layers (where reversal of the B-YIG layer changes the effective field experienced by the T-YIG layer) by estimating the magnetic coupling field H_{ex} needed to generate the observed resistance jump. The effective field on the T-YIG just before and after the B-YIG switching is $H_c - H_{ex}$ and $H_c + H_{ex}$, where H_c is the coercivity of the B-YIG and the net change in the effective field is $2H_{ex}$. Extrapolating the curve of the platinum resistance with magnetic field before the switching, we find that the net change of the effective field must reach over 40 Oe; that is, a magnetic coupling of at least 20 Oe is needed to explain the observed magnitude of the resistance jump (Fig. 3d). A more detailed evaluation of the magnetic coupling is provided in Supplementary Section 2.

To assess whether such a strong coupling is possible, minor SSE loops were measured (Fig. 3e). The H_c of the B-YIG can be obtained from different minor loops from the rate of the SSE signal with respect to the magnetic field, dV_{SSE}/dH_y (Fig. 3f). The offset field (H_b) of the minor loops for the B-YIG was identified as $(H_{c+} + H_{c-})/2$. Non-zero H_b represents coupling due to either the exchange bias with NiO or from the magnetic coupling with the T-YIG. The contribution to H_b due to the magnetic coupling and due to the exchange bias does and does not, respectively, depend on the initial direction of the T-YIG. By analysing the H_b data, we find the coupling field experienced by the B-YIG (T-YIG) is −1.8 Oe (−3.2 Oe), which is about one order of magnitude smaller than that required to produce the MNSMR signal discussed earlier. Antiferromagnetic $H_b = -3.4$ Oe of the B-YIG was also determined by minor loops of M–H hysteresis at 100 K (Supplementary Section 3). To further highlight the

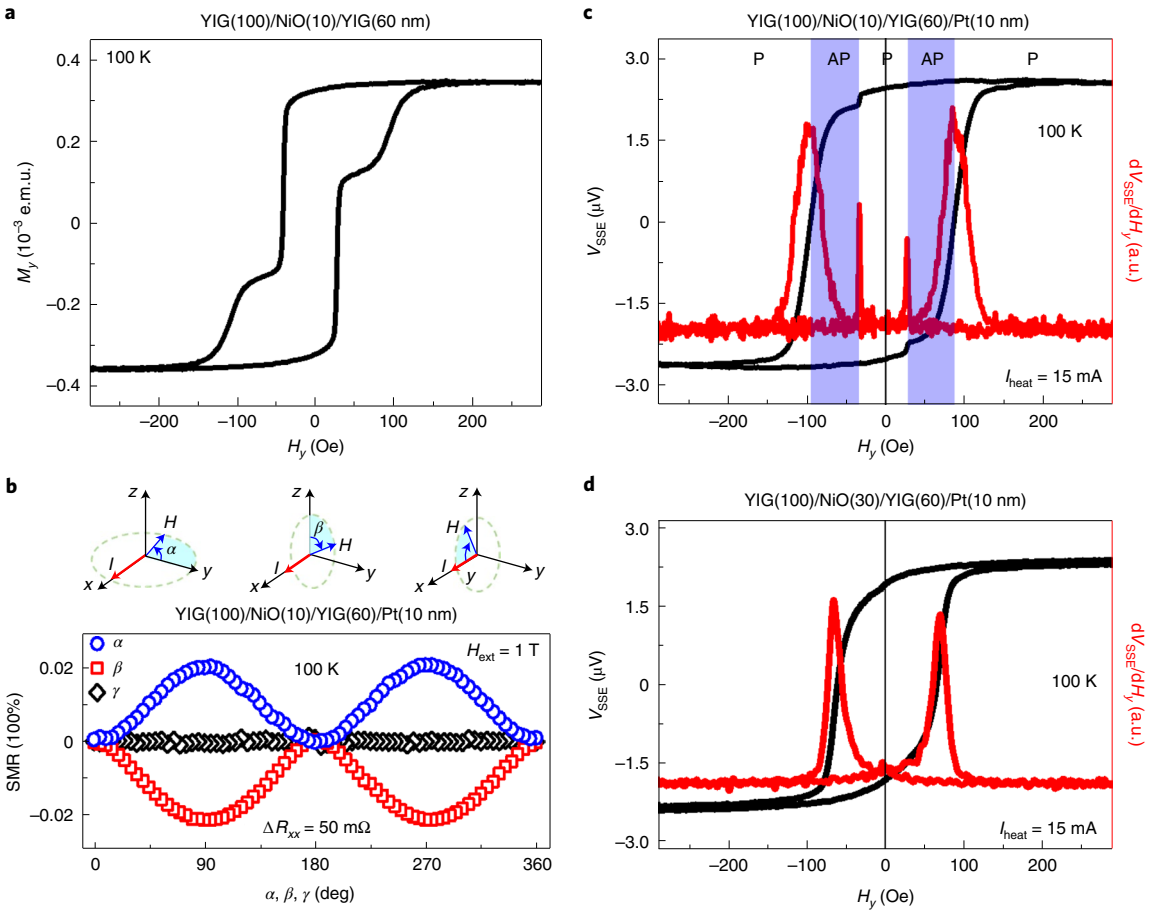

Fig. 2 | Magnetic and SSE characteristics of the MJ. a, M_y–H_y hysteresis (M_y, magnetization) of a YIG/NiO(10 nm)/YIG magnon junction. **b**, SMR measurement of the MJ/Pt system. $\Delta R \equiv R(\text{angle}) - R(\text{angle} = 0)$. A 1 T field was applied to saturate the magnetization of the YIG layers along the field direction. **c**, Spin Seebeck voltage V_{SSE} (black) and its field differential dV_{SSE}/dH_y (red) of the MJ as a function of H_y. **d**, V_{SSE} and dV_{SSE}/dH_y results for a YIG/NiO(30 nm)/YIG MJ with a thicker NiO spacer layer.

influence of any possible magnetic coupling, we measured the SSE and magnon magnetoresistance of a GGG//YIG(100)/SiO_2(10)/YIG(60)/Pt(10 nm) structure, which fully blocks any magnon current. The control sample only exhibited spin Seebeck voltage and ordinary SMR from the T-YIG (Supplementary Section 4). These results all indicate that magnetic coupling is not responsible for the resistance jump at H_c of the B-YIG.

We also measured the magnetoresistance at different currents and found no dependence on current polarity and magnitude (Supplementary Section 5), indicating neither heating nor unidirectional magnetoresistance[31] as possible origins of the abnormal resistance jump at H_c of the B-YIG in Fig. 3a. Furthermore, an MNSMR effect is observed at different temperatures, from 25 K to 325 K, in the YIG/NiO/YIG/Pt MJs (Supplementary Section 6), as well as in other material systems when tested in YIG/CoO/YIG/Pt and YIG/Au/YIG/Pt structures (Supplementary Section 7), indicating that the MNSMR effect is a universal phenomenon of magnon valves. The SMR measured at 100 K is also insensitive to field-cooling protocols, probably due to the very low blocking temperature of 15 K for the interface between NiO and B-YIG (Supplementary Section 8).

Phenomenological model of MNSMR

We propose that the observed resistance jump is due to the magnon valve effect, where the resistance of the platinum layer depends on the magnetic configuration of both top and bottom YIG layers. The spin current from the platinum layer converts to the magnon current at the interface, subsequently propagates into the insulating MJ and finally decays in it. During this process, the spin relaxation rates in different parts of the layers control the steady-state spin accumulation at the interface. If we introduce an effective spin-magnon conductance at the interface, G_s, and an effective magnon conductance of the MJ, G_{mj}, we may approximately connect the spin current at the two sides of the interface between Pt and the T-YIG via the spin current continuity equation:

$$\theta j_e - D\frac{\partial \mu}{\partial x} = \left(G_s^{-1} + G_{mj}^{-1}\right)^{-1}\mu$$

where θ is the spin Hall angle and D is the diffusion constant of Pt, j_e is the electric current density and μ is the spin chemical potential (or spin accumulation) at the interface. Assuming a simple exponential form of the chemical potential, $\frac{\partial \mu}{\partial x} = \frac{\mu}{\lambda}$, the above equation leads to the spin accumulation:

$$\mu = \frac{\theta j_e}{D\lambda^{-1} + G_t}$$
$$G_t^{-1} = (G_s^{-1} + G_{mj}^{-1})$$

The effective magnon conductance G_{mj} depends on the entire MJ configuration, which gives rise to a different value for the P and AP states. Our experimental result requires that the effective G_{mj} is larger for the AP state than for the P state.

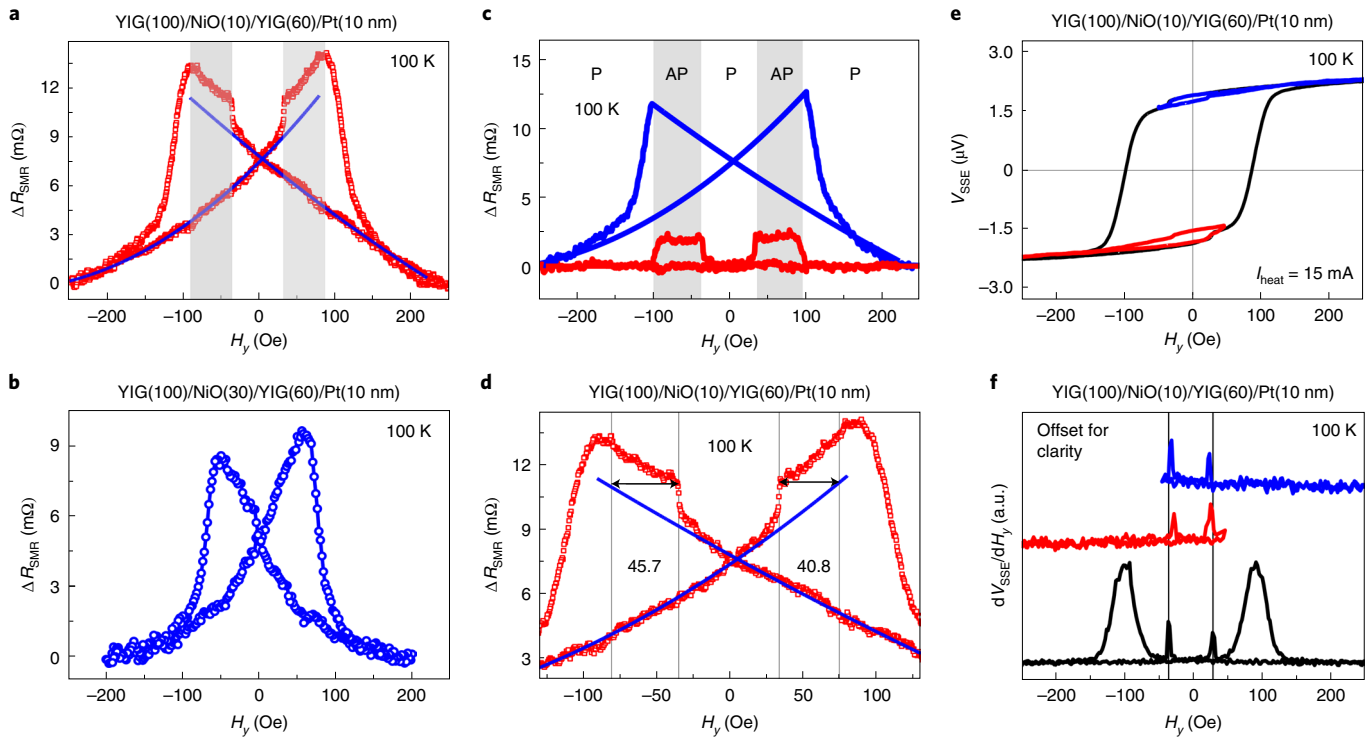

Fig. 3 | MNSMR of the MJ. a,**b**, The SMR in the YIG/NiO(10 nm)/YIG/Pt MJ (**a**) and in the YIG/NiO(30 nm)/YIG/Pt control sample (**b**). A resistance jump at H_c of the B-YIG is present in **a** but absent in **b**. Here $\Delta R \equiv R(H_y) - R(-250\,\text{Oe})$. Shaded regions represent AP states. **c**, The resistance in **a** is decomposed into two parts: the blue component shows the conventional SMR of the T-YIG/Pt and the red component is the MNSMR due to reversal of the B-YIG. **d**, Magnified MR around the H_c of the B-YIG to obtain the required coupling field if the resistance jump came from a trivial magnetic coupling effect between the two YIG layers. **e**,**f**, V_{SSE} (**e**) and dV_{SSE}/dH_y (**f**) of the minor loops of the YIG/NiO(10 nm)/YIG/Pt MJ as a function of applied field H_y. Blue and red curves denote negative and positive initialization of the T-YIG, respectively. The corresponding data of the full loop (black) are also shown for comparison. All data in this figure were measured at 100 K.

Although the above simple model could qualitatively explain our observation, a quantitative comparison between theory and experiment would involve detailed transport of thermal magnons in the MJ. If the magnon diffusion model is used for each layer in the MJ, we find that G_{mj} is always larger for the P state, similar to the spin diffusion model for electron spins in the conventional metallic spin valve and magnetic tunnel junction that yields a larger spin conductance for the P state. To interpret the smaller effective magnon conductance G_{mj} for the P state in the MJ than for the AP state, the theory must be extended beyond the simple magnon diffusion approach. The result $G_{mj,AP} > G_{mj,P}$ can be interpreted in another way by treating the B-YIG/NiO/T-YIG MJ, as a whole, as a single magnon sink. At the steady state, injected magnon current across the Pt/T-YIG interface should be equal to the non-equilibrium magnon relaxation rate inside the MJ. The result $R_{AP} > R_P$ means that the MJ in the AP state has a stronger magnon relaxation capability than in the P state. The stronger magnon relaxation may result from stronger magnon scattering for the AP state. Further theoretical investigations are needed to better understand the microscopic magnon scattering and relaxation mechanisms inside MJs.

Conclusions

We have reported a magnetoresistance in platinum/MJ heterostructures. In contrast to SMR, this MNSMR comes from magnon conductance across the MJ and is dependent on the orientation of both the top and bottom YIG layers, with the AP state having a higher effective conductance value than the P state. The higher magnon current reduces the spin accumulation at the platinum interface, leading to a higher inverse SHE opposed to the current and a higher resistance. MNSMR is a nonlocal spin transport effect where the electron transport is limited to the platinum layer, whereas the magnetic configuration change occurs in an entirely insulating YIG/NiO/YIG MJ. Analogous to TMR and GMR devices, this magnon-based magnetoresistance could potentially be used in spintronic and magnonic devices to control spin/magnon current, but without Joule heating, and could thus provide superior energy efficiencies.

Methods

The MJ stacks (YIG(100)/NiO(10)/YIG(60 nm) and YIG(100)/CoO(10)/YIG(60 nm)) and the magnon valve stack (YIG(40)/Au(10)/YIG(20 nm)) were deposited on $Gd_3Ga_5O_{12}$ (GGG) (111) substrates in a sputtering system (ULVAC-MPS-4000-HC7 model) with a base vacuum of 1×10^{-6} Pa. After deposition, high-temperature annealing was carried out to further improve the crystalline quality of the YIG layers. A 10 nm platinum stripe (100 μm × 1,000 μm lateral dimensions) for SSE and SMR measurements was fabricated by standard photolithography combined with an argon-ion dry-etching process. Finally, an insulating SiO_2 layer (100 nm) and a Pt/Au stripe were successively deposited on top of the Pt stripe for on-chip heating. Before platinum deposition, *M*–*H* hysteresis was measured with a vibrating sample magnetometer (VSM, EZ-9 from MicroSense). After the microfabrication process, all electrical measurements were performed in a physical property measurement system (PPMS-9T, Quantum Design) with magnetic fields of up to 9 T and temperatures down to 1.8 K. A Keithley 2400 instrument provided a heating current I_{heat} to the Pt/Au stripe for SSE measurements, as in ref. [16], or provided a current I along the x axis in the platinum stripe for SMR measurements (Fig. 1a). A Keithley 2182 instrument was used to pick up a voltage along the platinum stripe in both the SSE and SMR measurements. A magnetic field was applied along the transverse direction (along the y axis) of the platinum stripe. Before measuring the SSE and SMR effects at 100 K, the device was first cooled to 10 K from 300 K under H_y of −350 Oe and the temperature was increased to 100 K for the measurements. The SMR data at 100 K weakly depended on the field-cooling protocols (Supplementary Section 8), consistent with other reports about the insensitivity of spin transfer to exchange bias[16,32].

Data availability

The data that support the plots within this paper including the main text and Supplementary Information and other findings of this study are available from the corresponding author upon reasonable request.

Received: 29 August 2019; Accepted: 13 April 2020;

References

1. Baibich, M. N. et al. Giant magnetoresistance of (001)Fe/(001)Cr magnetic superlattices. *Phys. Rev. Lett.* **61**, 2472–2475 (1988).
2. Binasch, G., Grünberg, P., Saurenbach, F. & Zinn, W. Enhanced magnetoresistance in layered magnetic structures with antiferromagnetic interlayer exchange. *Phys. Rev. B* **39**, 4828–4830 (1989).
3. Miyazaki, T. & Tezuka, N. Giant magnetic tunneling effect in Fe/Al_2O_3/Fe junction. *J. Magn. Magn. Mater.* **139**, L231–L234 (1995).
4. Moodera, J. S., Kinder, L. R., Wong, T. M. & Meservey, R. Large magnetoresistance at room temperature in ferromagnetic thin film tunnel junctions. *Phys. Rev. Lett.* **74**, 3273–3276 (1995).
5. Wood, R. Future hard disk drive systems. *J. Magn. Magn. Mater.* **321**, 555–561 (2009).
6. Huai, Y., Albert, F., Nguyen, P., Pakala, M. & Valet, T. Observation of spin-transfer switching in deep submicron-sized and low-resistance magnetic tunnel junctions. *Appl. Phys. Lett.* **84**, 3118–3120 (2004).
7. Fuchs, G. D. et al. Spin-transfer effects in nanoscale magnetic tunnel junctions. *Appl. Phys. Lett.* **85**, 1205–1207 (2004).
8. Cornelissen, L. J. et al. Nonlocal magnon–polaron transport in yttrium iron garnet. *Phys. Rev. B* **96**, 104441 (2017).
9. Nakata, K., Simon, P. & Loss, D. Spin currents and magnon dynamics in insulating magnets. *J. Phys. D* **50**, 114004 (2017).
10. Cornelissen, L. J. et al. Long-distance transport of magnon spin information in a magnetic insulator at room temperature. *Nat. Phys.* **11**, 1022–1026 (2015).
11. Wu, H. et al. Observation of magnon-mediated electric current drag at room temperature. *Phys. Rev. B* **93**, 060403 (2016).
12. Li, J. et al. Observation of magnon-mediated current drag in Pt/yttrium iron garnet/Pt (Ta) trilayers. *Nat. Commun.* **7**, 10858 (2016).
13. Lin, W. W. & Chien, C. L. Electrical detection of spin backflow from an antiferromagnetic insulator/$Y_3Fe_5O_{12}$ interface. *Phys. Rev. Lett.* **118**, 067202 (2017).
14. Lebrun, R. et al. Tunable long-distance spin transport in a crystalline antiferromagnetic iron oxide. *Nature* **561**, 222–225 (2018).
15. Qiu, Z. et al. Spin colossal magnetoresistance in an antiferromagnetic insulator. *Nat. Mater.* **17**, 577–580 (2018).
16. Guo, C. Y. et al. Magnon valves based on YIG/NiO/YIG all-insulating magnon junctions. *Phys. Rev. B* **98**, 134426 (2018).
17. Chumak, A. V. et al. Magnon spintronics. *Nat. Phys.* **11**, 453–461 (2015).
18. Wu, H. et al. Magnon valve effect between two magnetic insulators. *Phys. Rev. Lett.* **120**, 097205 (2018).
19. Uchida, K. et al. Spin Seebeck insulator. *Nat. Mater.* **9**, 894–897 (2010).
20. Uchida, K. et al. Observation of longitudinal spin-Seebeck effect in magnetic insulators. *Appl. Phys. Lett.* **97**, 172505 (2010).
21. Cramer, J. et al. Magnon detection using a ferroic collinear multilayer spin valve. *Nat. Commun.* **9**, 1089 (2018).
22. Wright, K. Focus: a trio of magnon transistors. *Physics* **11**, 23 (2018).
23. Cornelissen, L. J., Liu, J., van Wees, B. J. & Duine, R. A. Spin-current-controlled modulation of the magnon spin conductance in a three-terminal magnon transistor. *Phys. Rev. Lett.* **120**, 097702 (2018).
24. Das, K. S., Liu, J., van Wees, B. J. & Vera-Marun, I. J. Efficient injection and detection of out-of-plane spins via the anomalous spin Hall effect in permalloy nanowires. *Nano Lett.* **18**, 5633–5639 (2018).
25. Das, K. S., Feringa, F., Middelkamp, M., van Wees, B. J. & Vera-Marun, I. J. Modulation of magnon spin transport in a magnetic gate transistor. *Phys. Rev. B* **101**, 054436 (2020).
26. Hirsch, J. E. Spin Hall effect. *Phys. Rev. Lett.* **83**, 1834–1837 (1999).
27. Zhang, S. F. Spin Hall effect in the presence of spin diffusion. *Phys. Rev. Lett.* **85**, 393–396 (2000).
28. Nakayama, H. et al. Spin Hall magnetoresistance induced by a nonequilibrium proximity effect. *Phys. Rev. Lett.* **110**, 206601 (2013).
29. Kim, J., Sheng, P., Takahashi, S., Mitani, S. & Hayashi, M. Spin Hall magnetoresistance in metallic bilayers. *Phys. Rev. Lett.* **116**, 097201 (2016).
30. Shan, J. et al. Influence of yttrium iron garnet thickness and heater opacity on the nonlocal transport of electrically and thermally excited magnons. *Phys. Rev. B* **94**, 174437 (2016).
31. Avci, C. O. et al. Unidirectional spin Hall magnetoresistance in ferromagnet/normal metal bilayers. *Nat. Phys.* **11**, 570–575 (2015).
32. Saglam, H. et al. Independence of spin–orbit torques from the exchange bias direction in $Ni_{81}Fe_{19}$/IrMn bilayers. *Phys. Rev. B* **98**, 094407 (2018).

Acknowledgements

This work was supported by the National Key Research and Development Program of China (MOST, grant nos 2017YFA0206200 and 2016YFA0300802) and the National Natural Science Foundation of China (NSFC, grant nos 51831012, 51620105004, 11974398, 51701203 and 11674373) and partially supported by the Strategic Priority Research Program (B) (grant no. XDB07030200), the International Partnership Program (grant no. 112111KYSB20170090) and the Key Research Program of Frontier Sciences (grant no. QYZDJ-SSW-SLH016) of the Chinese Academy of Sciences (CAS). C.H.W acknowledges financial support from the Youth Innovation Promotion Association, CAS (2020008). We also thank X.-G. Zhang at the University of Florida for fruitful discussions.

Author contributions

X.F.H. led and was involved in all aspects of the project. C.H.W. and C.Y.G. are the first authors. C.Y.G., C.H.W., W.Q.H., M.K.Z. and Y.W.X. deposited stacks and fabricated devices. C.Y.G., C.H.W. and X.W. conducted magnetic and transport property measurements. C.H.W., Z.R.Y., S.Z. and P.T. contributed to modelling and theoretical analysis. C.H.W., S.Z. and X.F.H. wrote the paper. Z.R.Y., Y.Z.L. and Y.W.L. conducted the MuMax simulation. X.F.H. and C.H.W. supervised and designed the experiments. All authors contributed to data mining and analysis.

Competing interests

The authors declare no competing interests.

Additional information

Supplementary information is available for this paper at https://doi.org/10.1038/s41928-020-0425-9.

Correspondence and requests for materials should be addressed to X.F.H.

Reprints and permissions information is available at www.nature.com/reprints.

Publisher's note Springer Nature remains neutral with regard to jurisdictional claims in published maps and institutional affiliations.